Ocean wave transmission and reflection by viscoelastic ice covers

Article *in* Ocean Modelling · May 2015

Impact Factor: 2.93 · DOI: 10.1016/j.ocemod.2015.05.003

Xin Zhao

Clarkson University

Ocean Modelling 92 (2015) 1–10

Contents lists available at ScienceDirect

Ocean Modelling

journal homepage: www.elsevier.com/locate/ocemod

Ocean wave transmission and reflection by viscoelastic ice covers

Xin Zhao, Hayley H. Shen*

Department of Civil and Environmental Engineering, Clarkson University, Potsdam, NY 13699, USA

ARTICLE INFO

Article history:
Received 20 September 2014
Revised 15 May 2015
Accepted 17 May 2015
Available online 28 May 2015

Keywords:
Ice-covered oceans
Wave propagation
Viscoelastic
Transmission and reflection coefficients
Variational method

ABSTRACT

Modeling ice covers as viscoelastic continua, Zhao and Shen, (2013) applied a two-mode approximate method to determine the transmission and reflection between two different ice covers. This approximate solution considered only two modes of the dispersion relation. In addition, the horizontal boundary conditions were simplified by matching mean values over the interfaces. In this study, we employ a variational method (Fox and Squire, (1990)) to calculate the wave transmission and reflection from two connecting viscoelastic ice covers of different properties. The variational approach minimizes the overall error function at the interface of two ice covers, hence is more rigorous than the previous approximate method that minimized the difference between mean values at the interface. The effect of additional travelling and evanescent modes are also investigated. We compare results from different matching methods, as well as the effects of including additional modes. From this study, we find that additional modes do not always improve the results for our model. For all cases tested, two modes appear to be sufficient. These two modes represent the open-water-like and the elastic-pressure wave-like behavior. The two-mode approximate method and the variational method have similar results except at very short wave periods.

1. Introduction

Due to the rapid decrease of ice cover, wave conditions in the Arctic have intensified (Thomson and Rogers, 2014). In response to increased human activities, especially in the partially ice-covered region, wave models have begun including ice effects. For instance, WAVEWATCH III which used to treat ice covers as islands (Tolman, 2003) now includes three more options. In its latest release (Tolman et al., 2014, pp. 53–62), different physical processes are considered in these options: a constant attenuation rate, an eddy viscosity (Liu and Mollo-Christensen, 1988), and viscoelasticity (Wang and Shen, 2010), all rely on parameterization that awaits further theoretical and observational development. In this study we focus on further developing the viscoelastic theory which envisions an ice cover as a continuum with some elastic property that changes wave speed without damping its energy and viscous property that mainly consumes energy but may also contribute to wave speed change for high frequency components.

Real ice covers are inhomogeneous. Waves propagating between ice covers of different properties will transmit part of their energy and reflect the rest. Based on a thin-plate approach, this phenomenon has been studied extensively between open water and elastic plate and between different elastic plates (Squire, 2007, a review). Assuming that ice covers may be represented as a Voigt linear viscoelastic material, Wang and Shen (2011) studied this transmission/reflection problem between open water and an ice cover using a two-mode approximate method. This method was extended to transmission/reflection between two different ice covered regions in Zhao and Shen (2013). The two-mode approximate method included only two propagating modes closest to the open water waves and ignored all other propagating modes and all evanescent modes permitted by the dispersion relation. Furthermore, matching boundary conditions at the interface of two different regions were only carried out in an average sense.

The two-mode approximate method has the obvious advantage of being simpler and computationally faster than other methods that may include more modes and adopt a more rigorous matching method at the interface. However, its effect on the predicted transmission/reflection is uncertain until we compare the results with a better mathematical procedure that includes more admissible modes and treats the boundary conditions more rigorously. In this study, we examine the effect of including more modes that exist in the dispersion relation, including both propagating and evanescent modes. We also improve the matching criterion by using a variational method as in Fox and Squire (1990). We compare these new results with the two-mode approximate method, and previous studies that assumed ice covers as pure elastic materials.

The organization of this paper is as follows. Section 2 briefly outlines the theoretical formulation of the viscoelastic model. In Section 3, the variational method is presented. Section 4 gives the

* Corresponding author. Tel.: +1 315 268 7985.
E-mail address: hhshen@clarkson.edu (H.H. Shen).

http://dx.doi.org/10.1016/j.ocemod.2015.05.003
1463-5003/

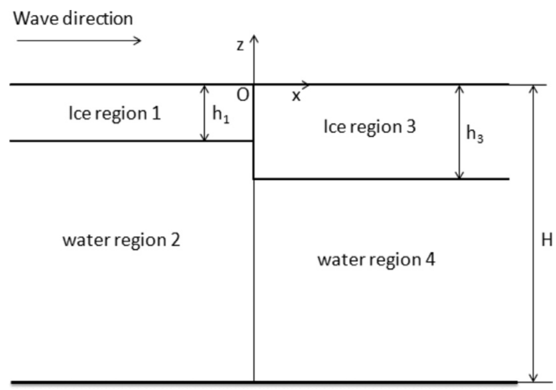

Fig. 1. Schematic of the coordinate frame of the problem.

result of special cases to compare with previous studies for pure elastic ice covers and the analysis on additional modes. Section 5 studies the energy partitions among three main propagating waves in elastic ice and viscous ice. The nature of these modes is also discussed. Section 6 provides details of the error analysis for the current method. The summary and conclusion are given in Sections 7 and 8 respectively. A linear wave regime is assumed in this study.

2. The theoretical formulation

2.1. Definition of the domain

The present study analyzes the same two-dimensional problem as in Zhao and Shen (2013). The sketch for the problem is shown in Fig. 1. The two ice covers are assumed to be fully submerged.

2.2. Governing equations, boundary conditions on horizontal surfaces, and the dispersion relation

In the present study, many more modes from the dispersion relation as derived in Wang and Shen (2010) will be included, hence for clarity, the derivation leading to the dispersion relation is briefly repeated here.

As previously done, for the ice cover we use a Voigt viscoelastic continuum model shown below

$$\tau_{mn} = -p\delta_{mn} + 2GS_{mn} + 2\rho_{ice}\nu\dot{S}_{mn}, \tag{1}$$

where ρ_{ice} is the density of the ice layer; τ_{mn}, S_{mn} and $\dot{S}_{mn}$ represent the stress tensor, the strain tensor and the strain rate tensor, respectively; m and n represent x or z; G and ν are the effective shear modulus and the effective kinematic viscosity of the ice layer, respectively; p is the pressure and δ_{mn} the Kronecker delta. For the regions occupied by an ice cover, either 1 or 3, the equation of motion is

$$\frac{\partial \mathbf{U}_i}{\partial t} = -\frac{1}{\rho_{ice}}\nabla p_i + \nu_{ei}\nabla^2\mathbf{U}_i + \mathbf{g}, \quad i = 1, 3, \tag{2}$$

where $\mathbf{U}_i = u_i\hat{e}_x + w_i\hat{e}_z$ is the velocity vector, $\mathbf{g}$ the gravitational acceleration,

$$\nu_{ei} = \nu_i + iG_i/\rho_{ice}\omega, \quad i = 1, 3, \tag{3}$$

is the viscoelastic parameter, and ω is the angular frequency of the incident wave. Using the decomposition with potential function ϕ and stream function ψ for the velocity (Lamb, 1932),

$$\mathbf{U}_i = -\nabla\phi_i + \nabla\times(0,\ \psi_i,\ 0), \quad i = 1, 3, \tag{4}$$

we obtain

$$\nabla^2\phi_i = 0, \tag{5}$$

$$\frac{\partial \psi_i}{\partial t} - \nu_{ei}\nabla^2\psi_i = 0, \tag{6}$$

$$\frac{\partial \phi_i}{\partial t} - \frac{p_i}{\rho_{ice}} - \Phi = 0, \quad i = 1, 3, \tag{7}$$

Here, $\Phi = gz$ is the gravitational potential.

For the associated water region below the ice covers 1 and 3, i.e. regions 2 or 4, we assume an inviscid fluid. The governing equations are

$$\frac{\partial \mathbf{U}_{i+1}}{\partial t} = -\frac{1}{\rho_{water}}\nabla p_{i+1} + \mathbf{g}, \tag{8}$$

$$\nabla^2\phi_{i+1} = 0, \tag{9}$$

$$\frac{\partial \phi_{i+1}}{\partial t} - \frac{p_{i+1}}{\rho_{water}} - \Phi = 0, \quad i = 1, 3. \tag{10}$$

The water velocity is related to the velocity potential only

$$\mathbf{U}_{i+1} = -\nabla\phi_{i+1}, \quad i = 1, 3. \tag{11}$$

Next we introduce the boundary conditions at the horizontal interfaces between air–ice, air–water, and water-sea floor. These conditions between regions 1 and 2 are identical to those between 3 and 4.

No stress at the air–ice interface

$$\tau_{xz,i} = \rho_{ice}\nu_{ei}\left(\frac{\partial u_i}{\partial z} + \frac{\partial w_i}{\partial x}\right) = 0,\ \tau_{zz,i} = -p_i + 2\rho_{ice}\nu_{ei}\frac{\partial w_i}{\partial z} = 0,\ z = 0,\ i = 1, 3. \tag{12}$$

Stress continuity at the ice–water interface

$$\tau_{zz,i} = -p_i + 2\rho_i\nu_{ei}\frac{\partial w_i}{\partial z} = \tau_{zz,i+1} = -p_{i+1},\ \tau_{xz,i} = \rho_{ice}\nu_{ei}\left(\frac{\partial u_i}{\partial z} + \frac{\partial w_i}{\partial x}\right) = 0,\ z = -h_i,\ i = 1, 3. \tag{13}$$

Kinematic condition at the air–ice interface

$$w_i = \frac{\partial \eta_i}{\partial t},\ z = 0,\ i = 1, 3. \tag{14}$$

Continuity of velocity at the ice–water interface

$$w_i = w_{i+1} = \frac{\partial \eta_{i+1}}{\partial t},\ z = -h_i,\ i = 1, 3. \tag{15}$$

No penetration condition at the sea floor

$$w_{i+1} = 0,\ z = -H,\ i = 1, 3. \tag{16}$$

In terms of the Fourier modes, the solutions are

$$\phi_i(x,\ z,\ t) = (A_i(n)\cosh k_i(n)z + B_i(n)\sinh k_i(n)z)e^{ik_i(n)x}e^{-i\omega t}, \tag{17}$$

$$\psi_i(x,\ z,\ t) = (C_i(n)\cosh\alpha_i(n)z + D_i(n)\sinh\alpha_i(n)z)e^{ik_i(n)x}e^{-i\omega t}, \tag{18}$$

for the ice region $i = 1, 3$, and

$$\phi_{i+1}(x,\ z,\ t) = E_i(n)\cosh k_i(n)(z + H)e^{ik_i(n)x}e^{-i\omega t}, \tag{19}$$

for the water region $i + 1 = 2, 4$. In the above, $\alpha_i^2(n) = k_i^2(n) - i\omega/\nu_{ei}$, $i = 1, 3$ and n indicates the n-th mode, as the dispersion relation to be shown has solutions, each one is an admissible mode. The no penetration condition at the sea floor is automatically satisfied by the cosh term in the potential and stream functions.

As shown in Appendix B in Zhao and Shen (2013), these boundary conditions together yield a set of homogeneous equations for $A_i(n)$, $B_i(n)$, $C_i(n)$, and $D_i(n)$ as shown below,

$$\begin{bmatrix} 0 & 2ik_i^2(n) & \alpha_i^2(n)+k_i^2(n) & 0 \\ -2ik_i^2(n)Sk_i^n & 2ik_i^2(n)Ck_i^n & (\alpha_i^2(n)+k_i^2(n))C\alpha_i^n & -(\alpha_i^2(n)+k_i^2(n))S\alpha_i^n \\ N_i^n\omega & -k_i(n)g & ik_i(n)g & L_i^n \\ -M_i^nSk_i^n+N_i^n\omega Ck_i^n & M_i^nCk_i^n-N_i^n\omega Sk_i^n & -iM_i^nC\alpha_i^n-L_i^nS\alpha_i^n & iM_i^nS\alpha_i^n+L_i^nC\alpha_i^n \end{bmatrix}\begin{bmatrix} A_i(n) \\ B_i(n) \\ C_i(n) \\ D_i(n) \end{bmatrix}=\begin{bmatrix} 0\\0\\0\\0\end{bmatrix} \quad (20)$$

which then solves for

$$E_i(n)=\frac{-A_i(n)Sk_i^n+B_i(n)Ck_i^n-iC_i(n)C\alpha_i^n+iD_i(n)S\alpha_i^n}{\sinh k_i(H-h_i)}. \quad (21)$$

In the above, $Sk_i^n=\sinh k_i(n)h_i$, $Ck_i^n=\cosh k_i(n)h_i$, $S\alpha_i^n=\sinh\alpha_i(n)h_i$, $C\alpha_i^n=\cosh\alpha_i(n)h_i$, $N_i^n=\omega+2i\nu_{ei}k_i^2(n)$, and $M_i^n=(\frac{\rho_{water}}{\rho_{ice}}-1)k_i(n)g-\frac{\rho_{water}}{\rho_{ice}}\frac{\omega}{\tanh(H-h_i)}$, and $L_i^n=2\nu_{ei}\omega k_i(n)\alpha_i(n)$.

The coefficients $A_i(n), B_i(n), C_i(n), D_i(n)$, and $E_i(n)$ are all complex numbers. The dispersion relation comes from setting the determinant of Eq. (20) to zero, which yields

$$Det=(\omega^2-Q_cgk\tanh kH)\frac{\omega^2}{\nu_e^2}\frac{\rho_{water}}{\rho_{ice}} \times\frac{4k^3\alpha\nu_e^2SkC\alpha+N^2S\alpha Ck-gkSkS\alpha}{\tanh kH}=0, \quad (22)$$

where

$$Q_c=1+\frac{\rho_{ice}}{\rho_{water}} \times\frac{g^2k^2SkS\alpha-(N^4+16k^6\alpha^2\nu_e^4)SkS\alpha-8k^3\alpha\nu_e^2N^2(C\alpha Ck-1)}{gk(4k^3\alpha\nu_e^2SkC\alpha+N^2S\alpha Ck-gkSkS\alpha)}. \quad (23)$$

Eq. (22) was simplified in Wang and Shen (2010) as

$$\omega^2=Q_cgk\tanh kH, \quad (24)$$

in order to most directly compare with open water, thin elastic plate, mass-loading, and two-layer viscous theories. The roots of the dispersion relation were, however, still calculated directly from the complete form of the determinant shown in Eq. (22). There are two more propagating roots and infinite symmetrical complex roots of this dispersion relation than those from the previously studied theories. As shown in Wang and Shen (2010), under proper limiting conditions, the dispersion relation converges to those from each of the previous theories.

2.3. Boundary conditions connecting different ice covered regions

We now proceed to determine the boundary conditions between two different viscoelastic regions representing ice covers of different properties. These are vertical interfaces between the two ice regions and the two water regions as shown in Fig. 1, we need to match the displacements, velocities, and stresses.

Water–Water interface: The boundary condition between water regions 2 and 4 includes continuity of the potential and the horizontal velocity

$$\phi_2(0,z)=\phi_4(0,z), \quad -H<z<-h_3; \quad (25)$$

$$\frac{\partial\phi_2(0,z)}{\partial x}=\frac{\partial\phi_4(0,z)}{\partial x}, \quad -H<z<-h_3. \quad (26)$$

Water–Ice interface: For the time being we assume $h_1<h_3$, the same analysis may be applied to other cases. Between water region 2 and ice region 3, the kinematic condition is

$$u_2(0,z)=u_3(0,z), \ -h_3<z<-h_1. \quad (27)$$

Likewise, the dynamical boundary condition is

$$\tau_{xx2}(0,z)=\tau_{xx3}(0,z), \ -h_3<z<-h_1. \quad (28)$$

These two conditions are the same as in Wang and Shen (2011) for wave propagating from open water to an ice covered region. In addition, we also include the continuity condition of shear stress at this interface

$$\tau_{xz3}(0,z)=0, \ -h_3<z<-h_1. \quad (29)$$

Ice–Ice interface: Between ice region 1 and ice region 3, we use the continuity conditions of horizontal and vertical velocities, and normal and shear stresses

$$u_1(0,z)=u_3(0,z), \ -h_1<z<0, \quad (30)$$

$$w_1(0,z)=w_3(0,z), \ -h_1<z<0; \quad (31)$$

$$\tau_{xx1}(0,z)=\tau_{xx3}(0,z), \ -h_1<z<0; \quad (32)$$

$$\tau_{xz1}(0,z)=\tau_{xz3}(0,z), \ -h_1<z<0. \quad (33)$$

In summary, the above nine equations, Eqs. (25–33), will be used to determine the transmission and reflection coefficients for a given wave. If freeboard is modeled instead of the current full submergence assumption, we will also need to include the stress free conditions over the exposed air-ice interface at $x=0$.

$$\tau_{xx}(0,z)=\tau_{xz}(0,z)=0, \ 0<z<h_{\text{freeboard}}. \quad (34)$$

These conditions are ignored at present.

3. Solutions

The variational method is developed to solve transmission and reflection coefficients from open water to a thin elastic plate (Fox and Squire, 1990). Using this method, Fox and Squire were able to examine the importance of matching boundary condition through the water depth instead of just at the free surface, as well as the inclusion of the two damped traveling modes and evanescent modes. Here, we extend the method to the viscoelastic model. This method is more rigorous than the two-mode approximate method used in Wang and Shen (2011). In the two-mode approximate method, we approximate all boundary conditions along the vertical interfaces by forcing the average values across the interface to be equal. In the variational method we minimize the differences across the entire interface. As in Fox and Squire (1990), we define the error function based on these boundary conditions as follows:

$$\begin{aligned}\varepsilon=\lambda_1&\int_{-H}^{-h_3}(\phi_2(0,z)-\phi_4(0,z))^2dz\\ &+\lambda_2\int_{-H}^{-h_3}(u_2(0,z)-u_4(0,z))^2dz\\ &+\lambda_3\int_{-h_1}^{0}(u_1(0,z)-u_3(0,z))^2dz\\ &+\lambda_4\int_{-h_1}^{0}(w_1(0,z)-w_3(0,z))^2dz\\ &+\lambda_5\int_{-h_1}^{0}(\tau_{xx1}(0,z)-\tau_{xx3}(0,z))^2dz\\ &+\lambda_6\int_{-h_1}^{0}(\tau_{xz1}(0,z)-\tau_{xz3}(0,z))^2dz\\ &+\lambda_7\int_{-h_3}^{-h_1}(u_2(0,z)-u_3(0,z))^2dz\end{aligned}$$

$$+\lambda_8\int_{-h_3}^{-h_1}(\tau_{xx2}(0,z)-\tau_{xx3}(0,z))^2dz$$
$$+\lambda_9\int_{-h_3}^{-h_1}\tau_{xz3}^2(0,z)dz, \qquad (35)$$

where $\{\lambda_n\}_{n=1}^{9}$ are the weighting factors which are chosen to improve the convergence. The key difference of the two-mode approximate method and the variational method is this error function. Let F_{iL}, F_{iR} be any property F_i at the left and right side of an interface, respectively. In the two-mode approximate method the error is defined as $\sum_i\int(F_{iL}-F_{iR})dz$ and in the variational method as $\sum_i\lambda_i\int(F_{iL}-F_{iR})^2dz$ where the integral is taken over the relevant interface along z. The error requirement is defined in Eq. (35). In addition, we will include more propagating modes than the two closest to the open water case as well as N evanescent modes to form the general solution. Other than evanescent modes, we will consider M propagating and complex modes. In the two-mode approximate method (Wang and Shen, 2011; Zhao and Shen, 2013), we included only two propagating modes and none of the evanescent modes. Thus, for the present study, the total potential function and the stream function may be written in terms of these $M+N$ modes as follows, where the individual modes are denoted by $n=1,2,\ldots,M+N$.

$$\phi_1(x,z,t)=I(1)(A_1(1)\cosh k_1(1)z$$
$$+B_1(1)\sinh k_1(1)z)e^{ik_1(1)x}e^{-i\omega t}$$
$$+\sum_{n=1}^{M+N}R(n)(A_1(n)\cosh k_1(n)z$$
$$+B_1(n)\sinh k_1(n)z)e^{-ik_1(n)x}e^{-i\omega t}; \qquad (36)$$

$$\psi_1(x,z,t)=I(1)(C_1(1)\cosh\alpha_1(1)z$$
$$+D_1(1)\sinh\alpha_1(1)z)e^{ik_1(1)x}e^{-i\omega t}$$
$$+\sum_{n=1}^{M+N}R(n)(C_1(n)\cosh\alpha_1(n)z$$
$$+D_1(n)\sinh\alpha_1(n)z)e^{-ik_1(n)x}e^{-i\omega t}; \qquad (37)$$

$$\phi_2(x,z,t)=I(1)E_1(1)\cosh k_1(1)(z+H)e^{ik_1(1)x}e^{-i\omega t}$$
$$+\sum_{n=1}^{M+N}R(n)E_1(n)\cosh k_1(n)(z+H)e^{-ik_1(n)x}e^{-i\omega t}; \qquad (38)$$

$$\phi_3(x,z,t)=\sum_{n=1}^{M+N}T(n)(A_3(n)\cosh k_3(n)z$$
$$+B_3(n)\sinh k_3(n)z)e^{ik_3(n)x}e^{-i\omega t}; \qquad (39)$$

$$\psi_3(x,z,t)=\sum_{n=1}^{M+N}T(n)(C_3(n)\cosh\alpha_3(n)z$$
$$+D_3(n)\sinh\alpha_3(n)z)e^{ik_3(n)x}e^{-i\omega t}; \qquad (40)$$

$$\phi_4(x,z,t)=\sum_{n=1}^{M+N}T(n)E_3(n)\cosh k_3(n)(z+H)e^{ik_3(n)x}e^{-i\omega t}; \qquad (41)$$

Here $I(1)$ is the amplitude of incident wave. The coefficients $A_i(n)$, $B_i(n), C_i(n), D_i(n), E_i(n)$ are solved with the singular value decomposition method. We then substitute them into the horizontal boundary conditions to form error function in terms of $I(1)$, $R(n)$, and $T(n)$. The error function contains $2(M+N)+1$ unknowns $I(1)$, $\{R(n)\}_{n=1}^{M+N}$, and $\{T(n)\}_{n=1}^{M+N}$. In vector form these unknowns are

$$\mathbf{u}=(I(1),\ R(1),\ R(2),\ldots R(M+N),\ T(1),\ T(2),\ldots,\ T(M+N))^T. \qquad (42)$$

The error function can be rewritten as follows:

$$\varepsilon=\mathbf{u}^T(\lambda_1\mathbf{Q}_1+\lambda_2\mathbf{Q}_2+\lambda_3\mathbf{Q}_3+\lambda_4\mathbf{Q}_4+\lambda_5\mathbf{Q}_5+\lambda_6\mathbf{Q}_6$$
$$+\lambda_7\mathbf{Q}_7+\lambda_8\mathbf{Q}_8+\lambda_9\mathbf{Q}_9)\mathbf{u}. \qquad (43)$$

The matrix $\mathbf{Q}_n$ is calculated analytically. To set the constraint of $I(1)=1$, we introduce a square matrix $\mathbf{K}$,

$$\mathbf{Ku}=\mathbf{v}. \qquad (44)$$

The elements of matrix $\mathbf{K}$ are all zero except $K_{1,1}=1$. The vector $\mathbf{v}$ contains coefficients corresponding to $I(1)=1$ and all others being zero. In all, these constraints can be written as follows:

$$\mathbf{u^TKu}-\mathbf{2v^Tu}+\mathbf{v}^T\mathbf{v}=0. \qquad (45)$$

Minimizing ε subject to the constraints (45) is performed by minimizing

$$\mathbf{u}^T(\lambda_1\mathbf{Q}_1+\lambda_2\mathbf{Q}_2+\lambda_3\mathbf{Q}_3+\lambda_4\mathbf{Q}_4+\lambda_5\mathbf{Q}_5+\lambda_6\mathbf{Q}_6$$
$$+\lambda_7\mathbf{Q}_7+\lambda_8\mathbf{Q}_8+\lambda_9\mathbf{Q}_9+\eta\mathbf{K})\mathbf{u}-2\eta\mathbf{v}^T\mathbf{u}. \qquad (46)$$

Here η is the weighting factor corresponding to the $I(1)=1$ constraint. Minimizing Eq. (46) is equivalent to solving the following:

$$\mathbf{Qu}=\eta\mathbf{v}, \qquad (47)$$

where

$$\mathbf{Q}=\lambda_1\mathbf{Q}_1+\lambda_2\mathbf{Q}_2+\lambda_3\mathbf{Q}_3+\lambda_4\mathbf{Q}_4+\lambda_5\mathbf{Q}_5+\lambda_6\mathbf{Q}_6$$
$$+\lambda_7\mathbf{Q}_7+\lambda_8\mathbf{Q}_8+\lambda_9\mathbf{Q}_9+\eta\mathbf{K}. \qquad (48)$$

By solving the inverse matrix of $\mathbf{Q}$, the coefficient vector $\mathbf{u}$ is obtained. With the continuity condition of the vertical displacement at the interface, we can derive the transmission and reflection coefficients for the surface profile.

$$R(n)=\frac{|R(n)||k_1(n)B_1(n)+ik_1(n)C_1(n)|}{|I(1)||k_1(1)B_1(1)-ik_1(1)C_1(1)|}; \qquad (49)$$

$$T(n)=\frac{|T(n)||k_3(n)B_3(n)-ik_3(n)C_3(n)|}{|I(1)||k_1(1)B_1(1)-ik_1(1)C_1(1)|}; \qquad (50)$$

where $n=1,2,..M$.

4. Results of wave transmission and reflection - pure elastic case

In this section we use the above solution procedure to study the behavior of wave propagation involving pure elastic ice covers. The results are compared with existing theories. For all cases shown, $\rho_{ice}=917\,\mathrm{kg/m^3}$, $\rho_{water}=1000\,\mathrm{kg/m^3}$, $H=100\,\mathrm{m}$. Based on the estimation of the magnitude for each error term, we choose the weighting factors as $\lambda_1=0.01$, $\lambda_2=\lambda_3=\lambda_4=\lambda_7=1$, $\lambda_5=\lambda_6=\lambda_8=\lambda_9=1/G_3^2$, and $\eta=1000$.

4.1. Between open water and elastic ice

We first consider the case of wave propagation from open water to an elastic ice cover. At this point we let $M=2$ and $N=0$, i.e. include only two propagating modes closest to the open water case as in Zhao and Shen (2013). The only change is that we adopt the new error function shown in Eq. (35). We thus focus on the effect of the more rigorous boundary matching criterion. Fig. 2 shows the reflected and transmitted coefficients defined in Eqs. (49, 50) with respect to the wave period for $\nu_{1,3}=0\,\mathrm{m^2/s}$, $G_1=0\,\mathrm{Pa}$, $G_3=1\,\mathrm{GPa}$, $h_1=0\,\mathrm{m}$, and $h_3=0.5\,\mathrm{m}$. The results compare the two-mode approximate method, the variational method, and a different model based on the thin elastic plate theory where the matched eigenfunction expansion method was used (Kohout et al., 2007). In their study 20 eigenmodes were included. However, due to the thin elastic plate assumption, they reduced the shear and bending boundary conditions at the interface to a point. Treatment of such boundary condition is closer to matching the mean values at the interface as done in Wang and Shen (2011).

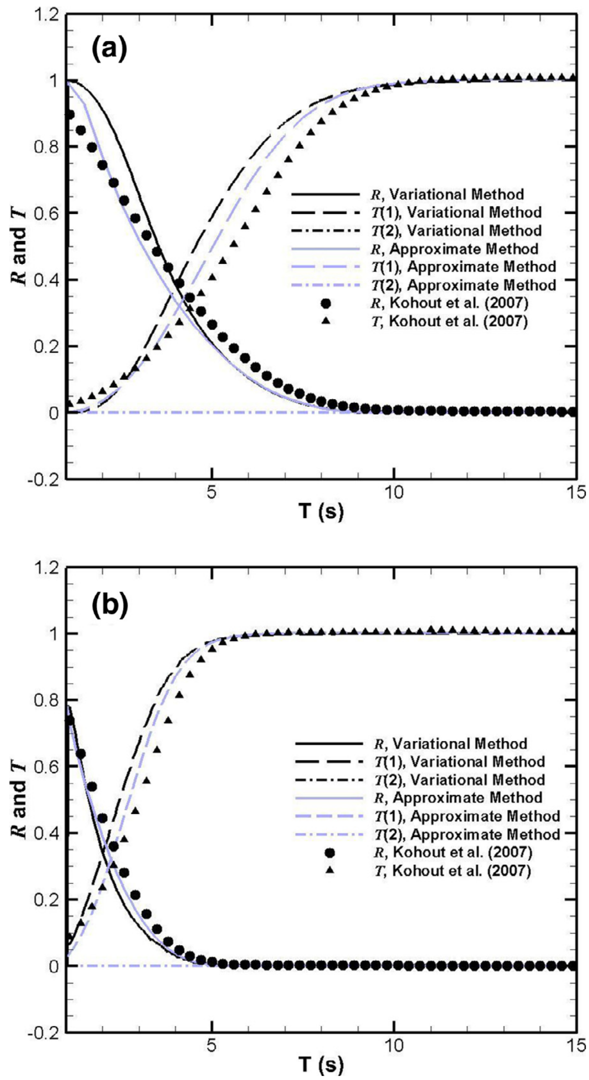

Fig. 2. Comparison between previous and the present studies of the reflection and transmission coefficients from open water to an elastic cover with respect to wave period. Here $\nu = 0\,\mathrm{m}^2/\mathrm{s}$ for both regions, $G_3 = 1\,\mathrm{GPa}$, and (a) $h_3 = 0.5\,\mathrm{m}$; (b) $h_3 = 0.1\,\mathrm{m}$. In this and the rest of the figures, $\rho_{ice} = 917\,kg/m^3$, $\rho_{water} = 1000\,kg/m^3$. (The dark and grey dash-dot lines coincide.).

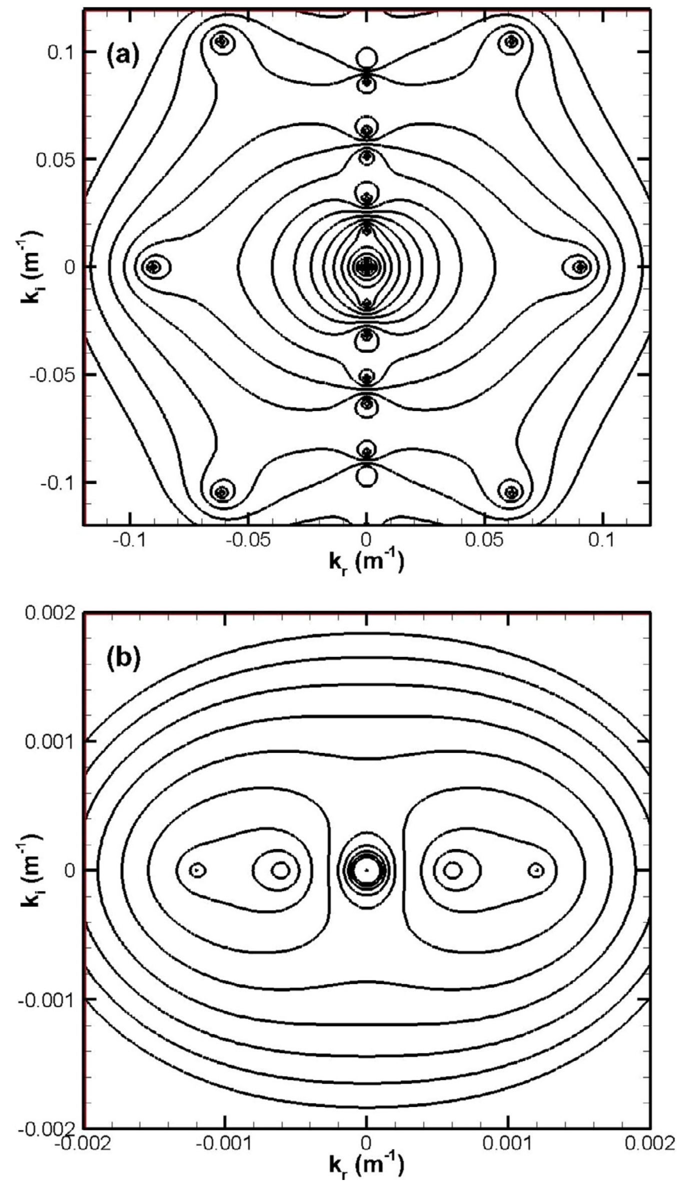

Fig. 3. Contour lines of the residual function $abs(Det)$. Here $\nu = 0\,\mathrm{m}^2/\mathrm{s}$, $G = 1\,\mathrm{GPa}$, and $h = 0.5\,\mathrm{m}$. (a) Wide-angle view where evanescent modes, two damped traveling modes, and the dominant mode on the real axis is seen near $k_r = 0.1\,\mathrm{m}^{-1}$; (b) Close-up view where the two modes on the real axis are seen.

Consequently Wang and Shen agreed better with Kohout et al. than the current results. Comparing Fig. 2a and b, all three cases converge to each other when h_3 reduces.

We next examine what happens if we include more modes. First we locate these modes in the complex k-space. Fig. 3 shows the map of contours of the residual function $abs(Det)$ defined by the full dispersion relation Eq. (22). The parameters used in Fig. 3 are the same as in Fig. 2. The “islands” of these contours are either poles or zeros of $abs(Det)$. The zeros are admissible roots of the dispersion relation. Unlike the thin elastic plate theory where only one real root exists, there are three roots on the real axis. These three roots approach the single one shown in the thin elastic plate theory if either the elasticity increases or the ice thickness decreases. In the approximate solution we included only two of these modes. We now expand this to include five modes: three on the real axis and one pair of symmetric damped travelling waves, Fig. 3a and b. We also examine the effect of evanescent modes, i.e. roots near the imaginary axis. We include 0, 10, and 100 of these modes. Fig. 4 shows the result of these different solutions. Fig. 4a compares results including two modes on the real axis, adding two damped travelling modes, then adding one more real root. It is seen that the effect of additional modes on the reflection and transmission coefficients is small for the present model. In fact, including additional complex and the 3rd modes seems to introduce fluctuations in the solution. From Fox and Squire (1990), the evanescent modes are required to obtain high accuracy solutions for thin elastic plate models. Fig. 4b shows the results of including only two real roots and different numbers of evanescent modes. The fluctuations of the solutions disappear. For the present model, two modes seem sufficient for the calculation of transmission and reflection coefficients. In the following discussions we keep only two modes and focus on comparing the approximate and variational methods. Detailed error analysis for the case shown in Fig. 4 is given in Section 6 when we return to this issue again.

4.2. Between arbitrary elastic ice covers

We now consider two linear elastic ice covers with different properties. This case has been studied by Barrett and Squire (1996) using the thin elastic plate theory and the variational method. First we

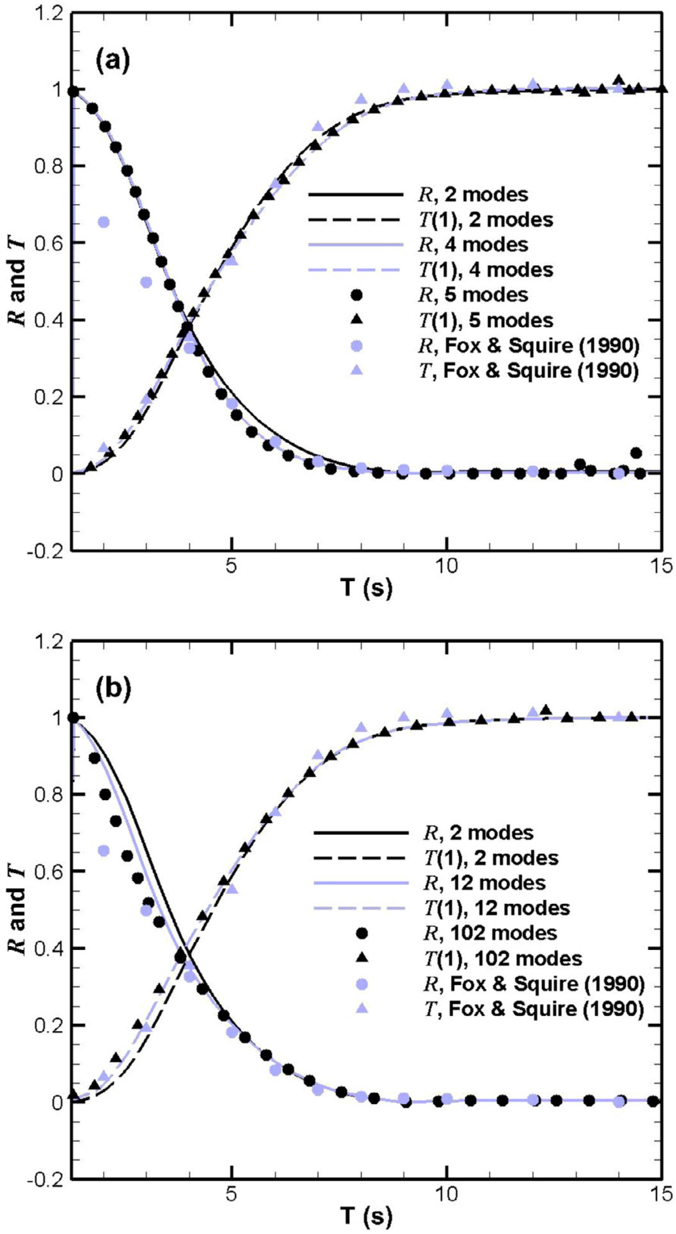

Fig. 4. Effect of including additional modes on transmission/reflection from open water to an elastic sheet with the same parameters as in Fig. 2. (a) 2 modes: include 2 propagating modes; 4 modes: add 2 symmetrical damped propagating modes; 5 modes: add 1 additional propagating mode. (b) 12 modes: add 10 evanescent modes to the 2 modes case. 102 modes: add 100 evanescent modes to the 2 modes case. Fox and Squire's results used 100 evanescent modes.

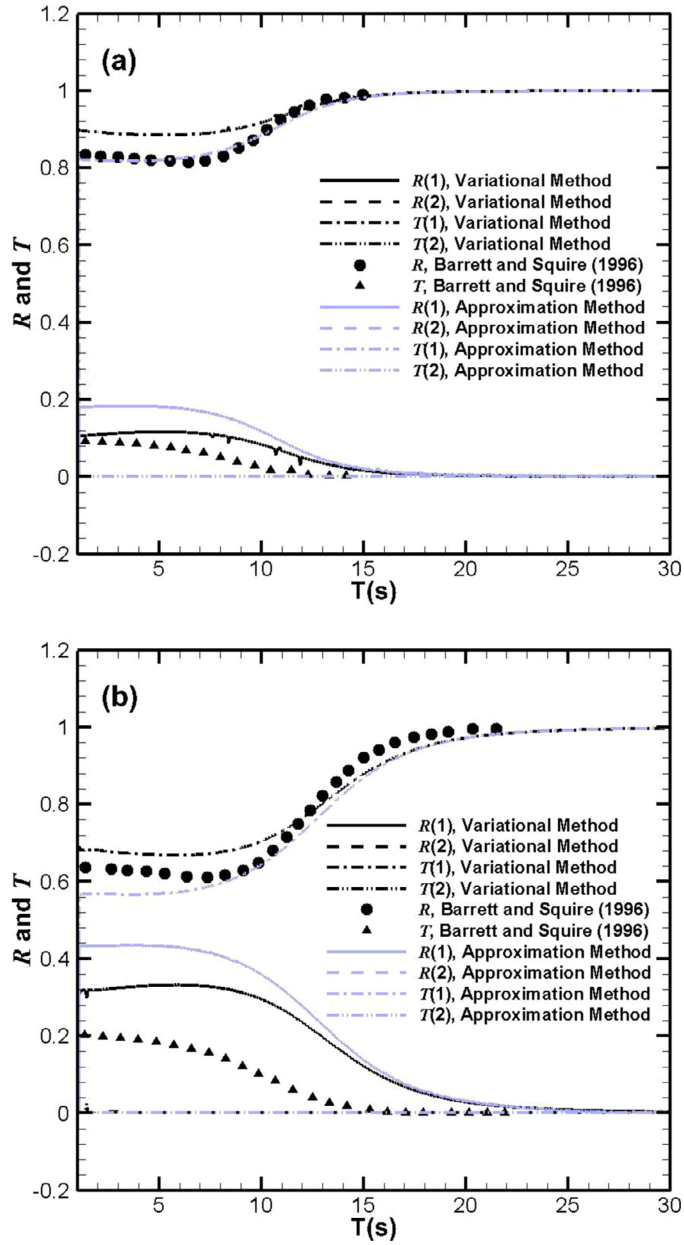

Fig. 5. Reflection and transmission coefficients with respect to wave period between two elastic ice regions with $\nu = 0\,\mathrm{m}^2/\mathrm{s}$ in both regions. (a) $G_1 = 2\,\mathrm{GPa}$, $G_3 = 5\,\mathrm{GPa}$, and $h_1 = h_3 = 1\,\mathrm{m}$; (b) $G_1 = G_3 = 5\,\mathrm{GPa}$, $h_1 = 1\,\mathrm{m}$, $h_3 = 2\,\mathrm{m}$. (In both cases, $R(2)$ and $T(2)$ are zero for both two-mode approximate method and variational method.).

present the case where the shear modulus differs between the two ice regions, all other parameters are identical. The results are shown in Fig. 5a. Next we examine the case when the ice thickness is different between the two regions, the rest of the parameters are identical. The results are shown in Fig. 5b. In each case, the reflection and transmission coefficients are qualitatively the same as in Barrett and Squire (1996) if their smoothly joined plate boundary conditions are used. The quantitative difference is substantial at short wave periods but diminishes at long periods. The difference is particularly noticeable for the reflection coefficient. This difference is caused by the continuum considerations used in the ice regions instead of the thin elastic plate assumption in Barrett and Squire (1996). Using the variational method to more strictly match the boundary condition does not consistently bring the two models closer to each other.

5. Energy partitions among modes in elastic ice and viscous ice

We now consider the energy partitions among three main modes and the “mode-switching” phenomenon as shown in Wang and Shen (2010, 2011) and Zhao and Shen (2013). Consider the case of wave propagating from open water to a pure elastic or pure viscous ice plate. In Fig. 6 we present the open water to pure elastic ice case by letting $h_1 = 0\,\mathrm{m}$, $h_3 = 0.5\,\mathrm{m}$, $\nu_3 = 0\,\mathrm{m}^2/\mathrm{s}$, $G_3 = 10^2 - 10^9\,\mathrm{Pa}$, $T = 6\,\mathrm{s}$. In this case the dispersion relation, Eq. (22), has three real roots. These are the main modes of the propagating waves. At low G one mode contains the majority of the transmitted energy. At high G the other does. The third mode which is included in the variational method but not the two-mode approximate method has negligible energy. Between the variational and two-mode approximate methods there is little difference of the resulting energy partition between the other

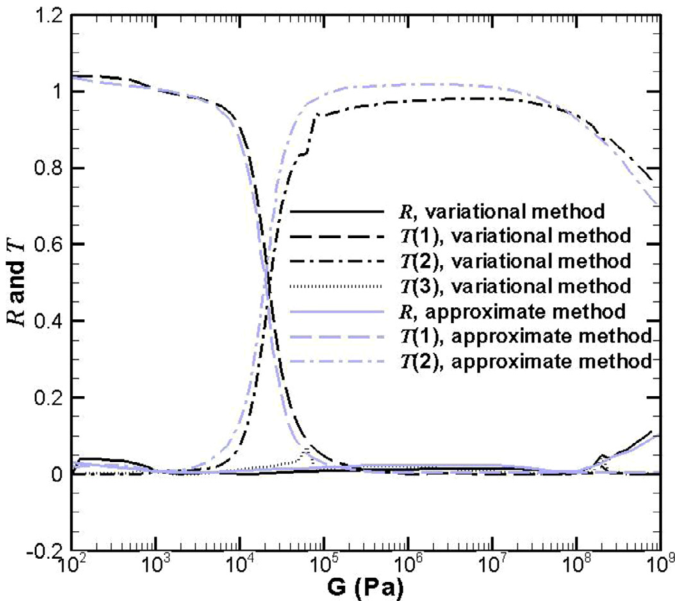

Fig. 6. Reflection and transmission coefficients with respect to shear modulus between open water and elastic ice with $h_3 = 0.5\,\text{m}$, $\nu_3 = 0\,\text{m}^2/\text{s}$, and $T = 6\,\text{s}$.

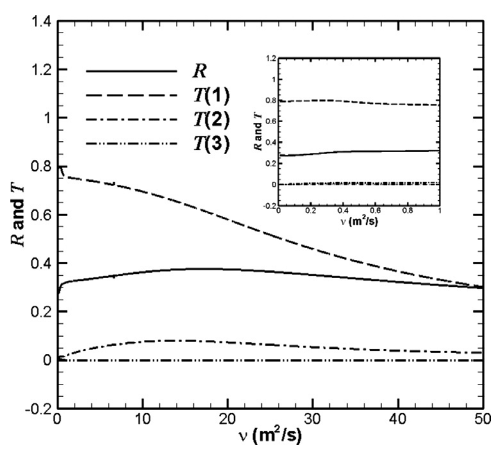

Fig. 7. Reflection and transmission coefficients with respect to viscosity between open water and viscous ice with $h_3 = 0.5\,\text{m}$, $G_3 = 0\,\text{Pa}$, and $T = 6\,\text{s}$.

two modes. The two dominant modes switch their energy partitions in the range from 10^4 Pa to10^5 Pa. Although the 3rd mode does contain some energy, it does not change the partition between the other two modes appreciably. In Fig. 7 we present the open water to pure viscous ice case by letting $h_1 = 0\,\text{m}$, $h_3 = 0.5\,\text{m}$, $\nu_3 = 0 - 50\,\text{m}^2/\text{s}$, $G_3 = 0\,\text{Pa}$, $T = 6\,\text{s}$. Because of the similarity, we present only those results from the variational method. Unlike the pure elastic ice case, increasing viscosity does not create a mode switch in energy partitions. With the increasing of viscosity, the reflected wave slightly increases its energy, while the transmitted waves decrease their energies. The mode closest to the open water solution always dominates the transmitted energy, and the second mode also has certain amount of energy. The third mode is negligible.

To further understand these modes, we examine them as a function of the shear modulus G. As an example, we solve the full dispersion relation defined in Eq. (22) for the case $T = 6\,\text{s}$, $\nu = 0\,\text{m}^2/\text{s}$ and obtain the three real roots in the contour map for each G. In Fig. 8 the behavior of the three modes are shown. Let them be ordered such that $k_{r1} \le k_{r2} \le k_{r3}$. As G increases from 0, in the beginning the first transmitted mode appears to follow that of the open water solution. The second mode has much greater wave number to begin

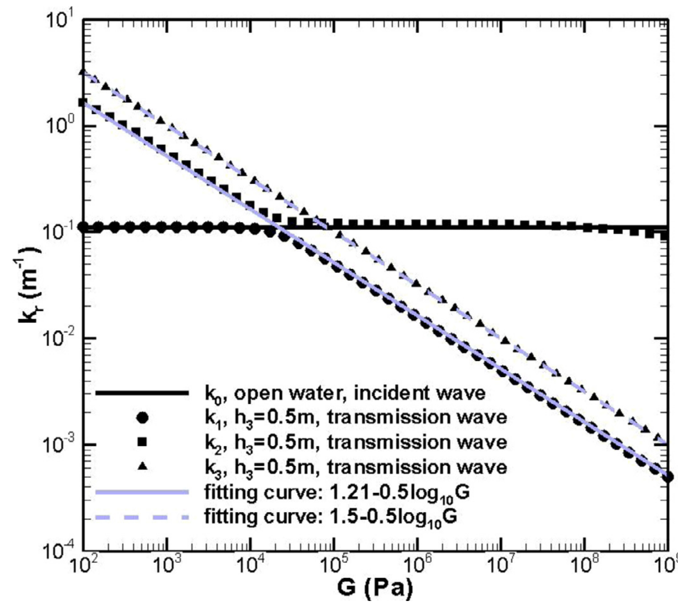

Fig. 8. Wave number of pure elastic ice with $\nu_3 = 0\text{m}^2/\text{s}$, T = 6 s and $h_3 = 0.5\,\text{m}$, $H = 100\ m$.

with, but approaches that of the open water as G increases. At around $G = 3 \times 10^4$ Pa for this case, both modes are close to each other. Further increasing G makes the first mode turn downward sharply to follow the trend of the second mode while the second mode turns to approach the open water case. Eventually as G becomes very large the second mode begins to drop and coincide with the thin elastic plate theory. All this time, the third mode constantly decreases. The third mode in this log–log plot is a straight line. Using these data we solve for its equation in the form of $k_r = aG^b$. It is found that $k_r = \omega\sqrt{\rho_{ice}/G}$ which is the elastic shear wave solution. The tangent to the asymptotes of the first and second mode is also well fitted by a straight line. Its best fit $k_r = aG^b$ yields $k_r = 16.2/\sqrt{G} \approx \omega\sqrt{\rho_{ice}/3G}$. Since we assumed that the ice cover is incompressible, its Poisson's ratio is 0.5 and the Young's modulus is $3G$, indicating that the nature of this branch of mode 1 or mode 2 is the elastic pressure wave. The above results are from a pure elastic case. This conclusion should hold for viscoelastic cases at least when the viscosity is not too large.

6. Error analysis

To see the contribution of error from each term shown in Eq. (35) we calculate

$$\varepsilon_i = \lambda_i \int_{z_l}^{z_u} (f_{left}(0, z) - f_{right}(0, z))^2 dz \tag{51}$$

where $i = 1$ to 9 and f_{left}, f_{right} are the corresponding function of the left and right side of the interface in the i-th term. The integration limits are z_l, $z_u$associated with each of the interfaces. λ_i is the i-th weighting factor defined in Section 4. We give the result of this analysis for the case shown in Fig. 4(b) only. Similar analysis was also done for the case shown in Fig. 5 with the same trend but much reduced errors. In this case, we have open water meeting an ice sheet, hence only five of the nine boundary conditions are needed. Fig. 9 shows the error terms defined in Eq. (51) for $i = 1, 2, 7, 8, 9$ for a range of wave period $T = 1 - 30\,\text{s}$. Except for terms 1 and 2 and at low period $T = 2\,\text{s}$, all other error terms are below 0.1% of incident wave amplitude with a general decreasing trend for longer periods. Fig. 10 examines the effect of including more modes in the solution for the worst case $T = 2\,\text{s}$, and compares that with $T = 5\,\text{s}$, and 12 s. It is seen that all terms except 1 and 2 are at a negligible level. The most significant error is from the first term. For this term with two modes, the error

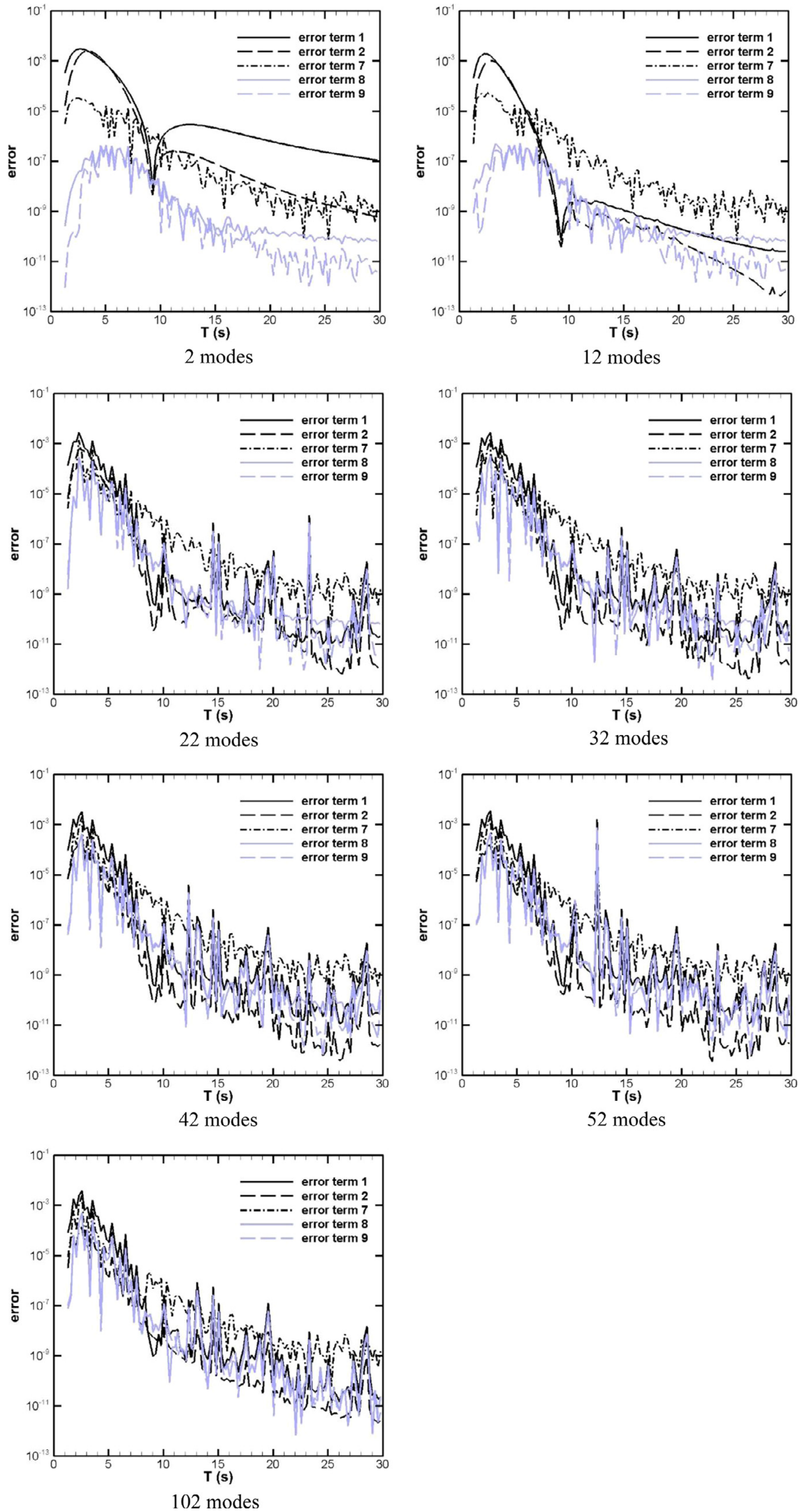

Fig. 9. Errors with different numbers of evanescent modes.

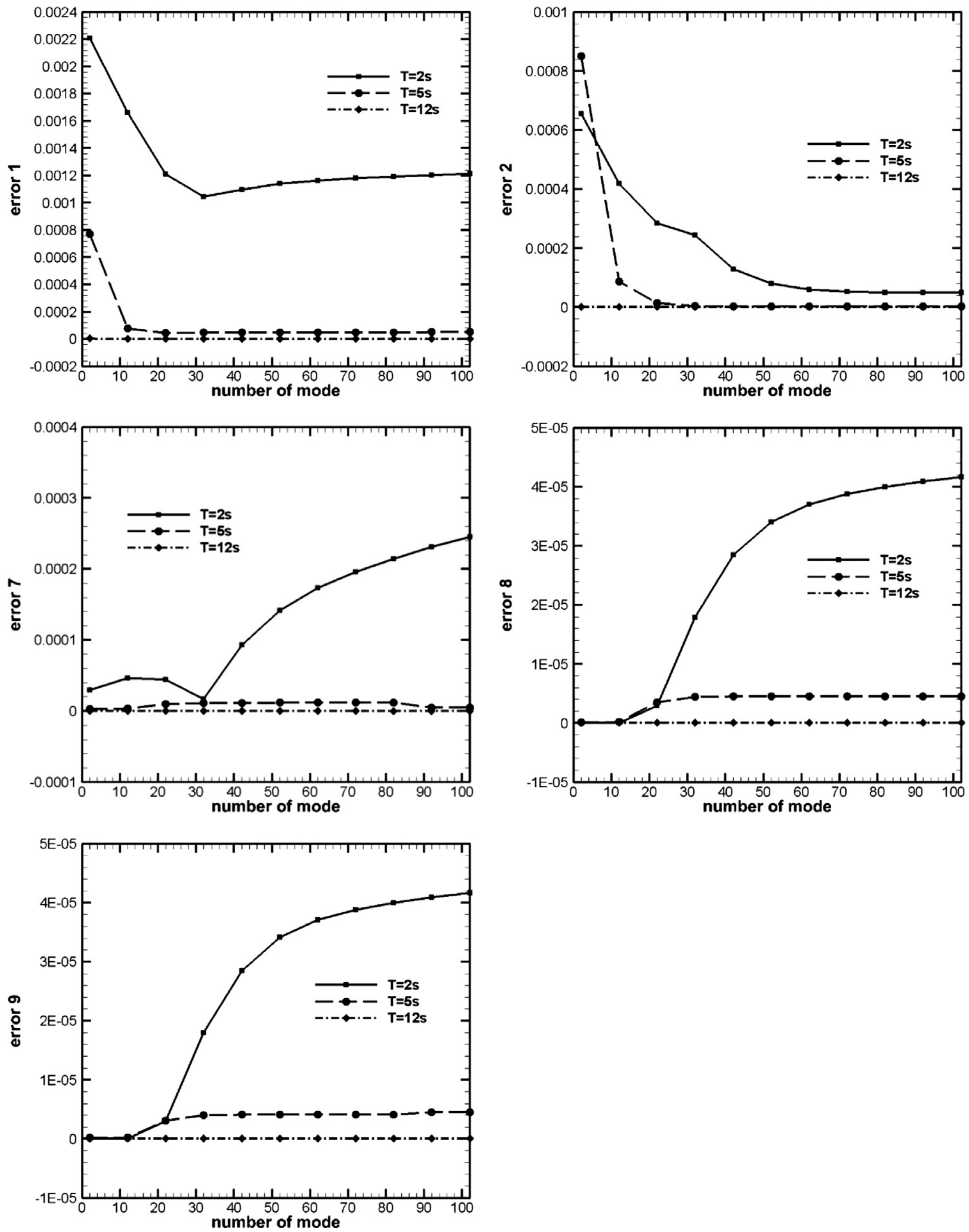

Fig. 10. Errors with respect to number of modes.

is slightly above 0.2%. By including 30 modes, the error drops to 0.1%. All errors are normalized by the incident wave amplitude.

7. Summary

We discuss the main findings of the present study which is based on assuming that ice covers are a viscoelastic continuum.

7.1. Comparison between different methods

Without changing the qualitative behavior, different methods do change the quantitative transmission/reflection between ice covers. This difference increases with the ice thickness (Fig. 2) due to the matching conditions at the interface: one uses the mean and the other minimizes the square differences. Between the thin elastic plate and the current solutions the differences come from a combination of boundary condition matching and the assumption of the constitutive behavior of the ice cover. This difference is less when the two-mode approximate method is used, because the boundary matching methods are close to each other.

7.2. Effect of damped travelling and evanescent modes

The viscoelastic dispersion relation has infinite damped travelling and evanescent modes. Upon examining the effect of including two damped travelling and different numbers of evanescent modes on the transmission/reflection coefficients, we find that the effect of these additional modes is small (Fig. 4). In fact, including two damped travelling modes and 3rd propagating mode for viscoelastic model introduces oscillations as shown in Fig. 4a. This situation is different from what was found from the thin elastic plate theory, in which Fox and Squire (1990) included two damped travelling modes without getting any numerical oscillations. From the error analysis of Section 6, if we require error $<0.1\%$, we need to include 20–30 evanescent modes. This is consistent with Fox and Squire (1990). In Fox and Squire (1990), the free-end boundary conditions at the ice edge are matched at a point, while in the present study the matching boundary conditions on velocity and stresses are matched over the entire interface. While this may have caused the differences between thin elastic plate theory and the viscoelastic continuum model, more extensive study is required to truly understand the differences between these two models.

7.3. Energy partitions in three modes

As discussed in Wang and Shen (2010) and Zhao and Shen (2013) and Fig. 6 of the present study, there is a mode switching phenomenon associated with increasing G. That is, at low Gone of the three modes for the dispersion relation dominates, as G increases the other mode becomes dominant. This switching occurs when the third mode approaches the other two. In close examination of the nature of these three modes as shown in Fig. 3, the two dominant modes are from the simplified dispersion relation Eq. (24) and the third is from the remaining terms of Eq. (22). Figs. 6 and 7 show the partition of energy among these three roots. The third root contains little energy and thus can be dropped from further analysis.

7.4. A remark on the difference between pure viscous and pure elastic ice

An interesting and unexpected result is shown in Fig. 7. Even for viscous ice with small viscosity the reflection can be significant. For elastic ice, the rigidity has to be relatively high to have the same effect. Hence when we model wave propagation from open water to an ice zone, we need to carefully consider the reflection from viscous ice like grease or brash ice at the edge.

8. Conclusions

In conclusion, for practical applications of the present viscoelastic model, one can ignore the evanescent modes to save considerable computational time. Of the many other propagating modes, the two from the simplified dispersion relation are sufficient for representing the wave transmission/reflection. Between the two-mode approximate method and the variational method, there is no difference in the computational cost, hence the variational method is preferred to more accurately match the boundary conditions. We emphasize that further study of the dominant modes in the viscoelastic dispersion is needed. So far, we have found that for pure elastic plates the two modes from the simplified dispersion relation always switch their dominance as G increases. For pure viscous covers this mode switching depends on the water depth. In case of a full viscoelastic material, whether there is mode switching between these two modes depends on the viscosity, the elasticity, and the water depth.

Results of this study are based on the assumption that the ice cover behaves as a Voigt viscoelastic material. In such material the internal stress is the linear sum of the elastic component and the viscous component. There are other viscoelastic constitutive laws that can be adopted. The mathematical complexity increases with more complicated viscoelastic models. Future studies will be motivated when physical evidence shows a more complicated model is needed. The present study assumes that the ice cover is semi-infinite. In many field cases, bands of ice covers are present. Waves propagating through these finite spans of ice cover will experience transmission and reflection from both the leading and the trailing edges, with multiple reflection/transmission between them. For pure elastic covers, Meylan and Squire (1994) applied a thin-plate theory to solve the finite plate case and showed very interesting resonant behavior of the reflection and transmission coefficients. For viscoelastic materials, this more complicated boundary value problem awaits further study.

Acknowledgment

This work is supported in part by the Office of Naval Research Grant #N00014-13-1-0294. We thank S. Cheng who reproduced the Fox and Squire (1990) results for Fig. 4. The helpful comments from anonymous reviewers are greatly appreciated, particularly concerning the error analysis.

References

Barrett, M.D., Squire, V.A., 1996. Ice-coupled wave propagation across an abrupt change in ice rigidity, density, or thickness. J. Geophys. Res. 101 (C9), 20825–20832.
Fox, C., Squire, V.A., 1990. Reflection and transmission characteristics at the edge of shore fast sea ice. J. Geophys. Res. 95, 11629–11639.
Kohout, A.L., Meylan, M.H., Sakai, S., Hanai, K., Leman, P., Brossard, D., 2007. Linear water wave propagation through multiple floating elastic plates of variable properties. J. Fluids Struct. 23 (4), 649–663.
Lamb, S.H., 1932. Hydrodynamics. Dover, New York.
Liu, A.K., Mollo-Christensen, E., 1988. Wave propagation in a solid ice pack. J. Phys. Oceanogr. 18 (11), 1702–1712.
Meylan, M.H., Squire, V.A., 1994. The response of ice floes to ocean waves. J. Geophys. Res. 99 (C1), 899–900.
Squire, V.A., 2007. Of ocean waves and sea-ice revisited. Cold Reg. Sci. Technol. 49, 110–133.
Thomson, J., Rogers, W.E., 2014. Swell and sea in the emerging Arctic ocean. Geophys. Res. Lett. 41, 3136–3140. doi:10.1002/2014GL059983.
Tolman, H.L., 2003. Treatment of unresolved islands and ice in wind wave models. Ocean Modell. 5, 219–231.
Tolman, H.L., and the WAVEWATCH III® Development Group, 2014. User manual and system documentation of WAVEWATCH III® version 4.18, NOAA Technical Note, MMAB Contribution No. 316, 311 p.
Wang, R., Shen, H.H., 2010. Gravity waves propagating into an ice-covered ocean: a viscoelastic model. J. Geophys. Res. 115, C06024.
Wang, R., Shen, H.H., 2011. A continuum model for the linear wave propagation in ice-covered oceans: an approximate solution. Ocean Modell. 38, 244–250.
Zhao, X., Shen, H.H., 2013. Ocean wave transmission and reflection between two connecting viscoelastic ice covers: an approximate solution. Ocean Modell. 71, 102–113.